

# Nonlinear Iterative Projection Methods with Multigrid in Photon Frequency for Thermal Radiative Transfer

Dmitriy Y. Anistratov

*Department of Nuclear Engineering, North Carolina State University, Raleigh, NC 27695  
anistratov@ncsu.edu*

---

## Abstract

This paper presents nonlinear iterative methods for the fundamental thermal radiative transfer (TRT) model defined by the time-dependent multifrequency radiative transfer (RT) equation and the material energy balance (MEB) equation. The iterative methods are based on the nonlinear projection approach and use multiple grids in photon frequency. They are formulated by the high-order RT equation on a given grid in photon frequency and low-order moment equations on a hierarchy of frequency grids. The material temperature is evaluated in the subspace of the lowest dimensionality from the MEB equation coupled to the effective grey low-order equations. The algorithms apply various multigrid cycles to visit frequency grids. Numerical results are presented to demonstrate convergence of the multigrid iterative algorithms in TRT problems with large number of photon frequency groups.

*Keywords:* thermal radiative transfer, Boltzmann equation, high-energy density physics, iteration methods, multigrid methods, quasidiffusion method, variable Eddington factor

---

## 1. Introduction

Radiation transport is of fundamental importance for high-temperature phenomena in high-energy density physics, inertial confinement fusion, astrophysics etc [1, 2, 3]. High-energy photons interact with matter and play essential role in redistribution of energy in a physical system. The dynamics of the system is affected by absorption and emission of photons by matter leading to change in the material temperature. The propagation of photons and their interaction with matter is described by the Boltzmann radiative transfer (RT) equation in which the opacities and emission source term are highly nonlinear functions of the material temperature [4]. The basic thermal radiative transfer (TRT) model is defined by the RT equation and the material energy balance (MEB) equation. The material energy depends nonlinearly on temperature. The advanced model is formulated by the system of radiation hydrodynamics equations that includes conservation of mass and momentum equations accounting for the effects of radiation [5, 6].

The dimensionality of the TRT problem is driven by the specific intensity of radiation that depends on time, spatial position, direction of particle motion, and photon frequency. In a general geometry, it is a seven-dimensional function. The parameters of matter depend only on space and time and hence four independent variables. The TRT system of equations is approximated by implicit methods to avoid stability constraints on the time step size. This yields a complicated and large system of equations on the phase-space grid. At a time level, the RT equation can be solved deterministically by sweeping a spatial mesh in each discrete direction for a photon frequency group.

*Preprint submitted to Elsevier*

The costs of transport calculations depend on complexity of a transport discretization scheme and the degree of phase space resolution by the grid. The computational effort on the same spatial grid scales with increase in number of angular directions and frequency groups. The RT equation is tightly coupled to the MEB equation. Simple iterations between the RT and MEB equations converge very slow. It is necessary to apply efficient iterative techniques to reduce number of transport iterations that involve transport sweeps on the phase-space grid.

To solve the nonlinear TRT problem, the RT and MEB equations can be linearized with respect to temperature. This yields a modified high-order RT equation with pseudo-scattering in the phase space on every time step [7, 8]. To accelerate transport iterations associated with pseudo-scattering, fast iteration methods, such as, the diffusion-synthetic acceleration, grey transport acceleration, Krylov methods are used [8, 9, 10, 11, 12].

The nonlinear projection approach (NPA) is based on applying projection operators in angular and frequency variables to formulate a system of low-order equations for moments of the intensity [13, 14]. The low-order moment equations are closed with the high-order RT equation by means of prolongation operators and exact closures. The iteration methods for solving RT equation based on the NPA are the quasidiffusion (QD) method (aka Eddington Variable Factor (VEF) method), nonlinear diffusion acceleration, coarse-mesh finite differencing (CMFD) method, partial current-based CMFD,  $\alpha$ -weighted methods [13, 15, 16, 17, 18, 19, 20]. The NPA has been applied to TRT and radiation hydrodynamics problems [21, 22, 23, 24, 25, 26, 27, 28, 29].

A group of iterative algorithms for frequency-dependent radiative transfer use two frequency grids involving the grey low-order transport problem which is coupled to the MEB equation to estimate the material temperature during iterations [21, 25, 26, 29]. The grey low-order problem is derived by a nonlinear projection of multigroup moment equations in photon frequency using the group radiation energy density and fluxes to define grey coefficients. The computational methods based on the linearized high-order RT and MEB equations formulate a grey problem for the modified RT equation with pseudo-scattering using the grey opacities averaged with slowest converging error modes [8, 10, 11].

In this study, the TRT problems with large number of groups are considered. It has been demonstrated that iterative methods based on nonlinear projection and multiple grids in particle energy are efficient algorithms for particle transport problems [30, 31, 32, 33]. In this paper, we present new nonlinear iterative methods for TRT problems with multigrid in photon frequency. They are formulated by means of the high-order RT equation on a given grid in photon frequency and low-order QD equations on multiple frequency grids. The hierarchy of grids for the low-order equations always include (i) the given fine grid as the first one and (ii) the grid with one interval that covers the whole frequency range. The MEB equation is coupled to the low-order equations on the coarsest frequency grid, namely, to the grey low-order equations. As a result, the material temperature is evaluated in the subspace of the lowest dimensionality.

The remainder of the paper is organized as follows. In Sec. 2, the TRT problem is described. In Sec. 3, the multilevel QD (MLQD) method with two frequency grids is reviewed. In Sec. 4, the MLQD method with multiple grids in photon frequency is formulated in continuous form; different multigrid algorithms are presented. The discretization of equations of the MLQD method is formulated in Sec. 5. The numerical results are presented in Sec 6. In Sec. 7, we conclude with a brief discussion.

## 2. Thermal Radiative Transfer Problem

We consider the TRT model in one-dimensional slab geometry. It is defined by the frequency-dependent RT equation [5]

$$\frac{1}{c} \frac{\partial I}{\partial t}(x, \mu, \nu, t) + \mu \frac{\partial I}{\partial x}(x, \mu, \nu, t) + \sigma(\nu, T)I(x, \mu, \nu, t) = \sigma(\nu, T)B(\nu, T), \quad (1)$$

$$x \in [0, X], \quad \mu \in [-1, 1], \quad t \geq 0, \quad \nu \in [0, \infty),$$

and the MEB equation

$$\frac{\partial \varepsilon(T)}{\partial t} = \int_0^\infty \int_{-1}^1 \sigma(\nu, T) \left( I(x, \mu, \nu, t) - B(\nu, T) \right) d\mu d\nu \quad (2)$$

with the initial conditions

$$I|_{t=0} = I^0, \quad (3)$$

$$T|_{t=0} = T^0, \quad (4)$$

and the boundary conditions

$$I|_{x=0} = I^+, \quad \mu \in (0, 1], \quad (5a)$$

$$I|_{x=X} = I^-, \quad \mu \in [-1, 0). \quad (5b)$$

Here  $I_\nu$  is the specific intensity,  $T$  is the material temperature;  $\varepsilon$  is the material energy density;  $\sigma_\nu$  is the photon opacity;  $x$  is the spatial position;  $\mu$  is the directional cosine of particle motion;  $\nu$  is the photon frequency;  $t$  is time.

$$B(\nu, T) = \frac{4\pi h\nu^3}{c^2} \frac{1}{e^{\frac{h\nu}{kT}} - 1} \quad (6)$$

is the Planck black-body distribution function multiplied by  $2\pi$ , where  $h$  is the Planck's constant,  $c$  is the speed of light,  $k$  is the Boltzmann's constant. The TRT model (1) and (2) neglects material motion, scattering, heat conduction, and external sources. It is applicable in the case of the supersonic radiation wave [34].

To formulate discretization of the RT equation with respect to the frequency variable, we define the grid

$$\Omega_\nu = \{\nu_g, g \in \mathbb{N}(n_\nu + 1)\} \quad (7)$$

that divides the whole frequency range into discrete groups given by intervals  $\omega_g = [\nu_g, \nu_{g+1}]$ . Here  $n_\nu$  is the number of groups,  $\mathbb{N}(n_\nu + 1) = \{1, \dots, n_\nu + 1\}$ ,  $\nu_1 = 0$ , and  $\nu_{n_\nu+1} = \infty$  or some maximum value. The TRT model in the multigroup approximation is defined by the RT equation

$$\frac{1}{c} \frac{\partial I_g}{\partial t} + \mathcal{L}_g I_g = q_g, \quad g \in \mathbb{N}(n_\nu), \quad (8)$$

$$I_g|_{x=0} = I_g^+, \quad \mu > 0, \quad I_g|_{x=X} = I_g^-, \quad \mu < 0, \quad (9)$$

$$I_g|_{t=0} = I_g^0 \quad (10)$$

for the group intensity

$$I_g = \int_{\nu_g}^{\nu_{g+1}} I d\nu, \quad (11)$$

where

$$\mathcal{L}_g I_g \equiv \mu \frac{\partial I_g}{\partial x} + \sigma_{E,g} I_g, \quad (12)$$

$$q_g = \sigma_{B,g} B_g, \quad (13)$$

$$B_g = \int_{\nu_g}^{\nu_{g+1}} B d\nu. \quad (14)$$

The RT equation (8) for the group  $g$  is formulated by means of two different group opacities:

$$\sigma_{B,g}(T) = \frac{\int_{\nu_g}^{\nu_{g+1}} \sigma(\nu, T) B(\nu, T) d\nu}{\int_{\nu_g}^{\nu_{g+1}} B(\nu, T) d\nu}, \quad \sigma_{E,g}(T, T_r) = \frac{\int_{\nu_g}^{\nu_{g+1}} \sigma(\nu, T) B(\nu, T_r) d\nu}{\int_{\nu_g}^{\nu_{g+1}} B(\nu, T_r) d\nu} \quad (15)$$

averaged with the Planck spectrum function at the material temperature  $T$  and the effective temperature of radiation,  $T_r$ , respectively [23, 25, 26]. The multigroup form of the MEB equation is given by

$$\frac{\partial \varepsilon}{\partial t} = \sum_{g=1}^{n_\nu} \int_{-1}^1 (\sigma_{E,g} I_g - \sigma_{B,g} B_g) d\mu. \quad (16)$$

### 3. Nonlinear Projection Methods

#### 3.1. The Two-Level QD Method

To solve the TRT problem (8) and (16), we apply the nonlinear projection approach based on the QD (VEF) method [13, 15]. The two-level QD method on the given grid in photon frequency is formulated by means of projection in the angular variable and exact closures of the moment equations. The system of equations of this method consists of two parts: (i) the high-order RT equation and (ii) the multigroup low-order QD (LOQD) equations on the grid  $\Omega_\nu$  for the angular moments of the group intensity. The LOQD problem for the group radiation energy density

$$E_g(x, t) = \frac{1}{c} \int_{-1}^1 I_g(x, \mu, t) d\mu \quad (17)$$

and flux

$$F_g(x, t) = \int_{-1}^1 \mu I_g(x, \mu, t) d\mu \quad (18)$$

is defined by the moment equations

$$\frac{\partial E_g}{\partial t} + \frac{\partial F_g}{\partial x} + c \sigma_{E,g} E_g = 2 \sigma_{B,g} B_g, \quad (19a)$$

$$\frac{1}{c} \frac{\partial F_g}{\partial t} + c \frac{\partial (f_g E_g)}{\partial x} + \sigma_{R,g} F_g = 0, \quad (19b)$$

where

$$f_g = \frac{\int_{-1}^1 \mu^2 I_g d\mu}{\int_{-1}^1 I_g d\mu} \quad (20)$$

is the group QD (Eddington) factor that defines the exact closure for the LOQD equations. The boundary and initial conditions are given by [13, 21]

$$F_g|_{x=0} = (cC_g^-(E_g - E_g^{in+}) + F_g^{in+})|_{x=0}, \quad F_g|_{x=X} = (cC_g^+(E_g - E_g^{in-}) + F_g^{in-})|_{x=X}, \quad (21)$$

$$E_g|_{t=0} = E_g^0, \quad F_g|_{t=0} = F_g^0, \quad (22)$$

where

$$C_g^- = \frac{\int_{-1}^0 \mu I_g(0, \mu, t) d\mu}{\int_{-1}^0 I_g(0, \mu, t) d\mu}, \quad C_g^+ = \frac{\int_0^1 \mu I_g(X, \mu, t) d\mu}{\int_0^1 I_g(X, \mu, t) d\mu} \Big|_{x=X} \quad (23)$$

are the boundary QD factors that define the closure for the energy density and flux at the boundary of the spatial domain, and

$$E_g^\pm = \pm \frac{1}{c} \int_0^{\pm 1} I_g^\pm d\mu, \quad F_g^\pm = \pm \int_0^{\pm 1} \mu I_g^\pm d\mu, \quad (24)$$

$$E_g^0 = \frac{1}{c} \int_{-1}^1 I_g^0 d\mu, \quad F_g^0 = \int_{-1}^1 \mu I_g^0 d\mu. \quad (25)$$

The first moment equation (19b) is defined with the Rosseland group opacity

$$\sigma_{R,g}(T, T_r) = \frac{\int_{\nu_g}^{\nu_{g+1}} \frac{\partial B(\nu, T')}{\partial T'} \Big|_{T'=T_r} d\nu}{\int_{\nu_g}^{\nu_{g+1}} \frac{1}{\sigma(\nu, T)} \frac{\partial B(\nu, T')}{\partial T'} \Big|_{T'=T_r} d\nu}. \quad (26)$$

The LOQD equations can be written in the following general operator form:

$$\frac{\partial \mathbf{Y}_g}{\partial t} + \mathcal{M}_g \mathbf{Y}_g = \mathbf{Q}_g, \quad \mathbf{Y}_g = (E_g, F_g)^T, \quad g \in \mathbb{N}(n_\nu), \quad (27)$$

where the operator  $\mathcal{M}_g = \mathcal{M}_g[f_g, C_g^\pm, T]$ ,  $f_g = f_g[I_g]$ ,  $C_g^\pm = C_g^\pm[I_g]$ , and  $\mathbf{Q}_g = \mathbf{Q}_g[T]$ . To couple the MEB equation with the LOQD equations, it is cast in the multigroup form in terms of the group energy densities as follows:

$$\frac{\partial \varepsilon(T)}{\partial t} = \sum_{g=1}^{n_\nu} (c\sigma_{E,g}E_g - 2\sigma_{B,g}B_g). \quad (28)$$

In summary, the system of equations of the two-level QD method on the frequency grid  $\Omega_\nu$  is defined by Eqs. (8), (19), and (28). The main feature of this method is that the estimation of temperature is performed in the projected space by solving the MEB equation coupled to the multigroup LOQD equations.

Algorithm 1 describes elements of the iterative scheme for the two-level QD method at every time step. Here  $s$  is the index of transport iterations;  $j$  is the index of the time step. The first stage of the iteration algorithm is to update group opacities  $\sigma_{E,g}$ ,  $\sigma_{B,g}$  using the latest estimation of the temperature  $T^{(s)}$ . This defines the operator  $\mathcal{L}_g^{(s)} = \mathcal{L}_g[T^{(s)}]$ . On the second stage, the

multigroup high-order RT equations are solved to obtain the group intensities  $I_g^{(s)}$ . Then,  $I_g^{(s)}$  is used to compute the QD factors  $f_g[I_g^{(s)}]$  and  $C_g^\pm[I_g^{(s)}]$ . This defines the low-order operator  $\mathcal{M}_g^{(s)} = \mathcal{M}_g[f_g^{(s)}, C_g^{\pm(s)}, T^{(s)}]$ . On the next stage, the new estimation of temperature is calculated by solving the MEB equation coupled to the multigroup LOQD equations defined by the operator  $\mathcal{M}_g^{(s)}$ . Various numerical techniques can be applied to solve the nonlinear system of the multigroup LOQD and MEB equations on the frequency grid  $\Omega_\nu$ .

```

s = 0, T(1) = Tj-1
while ||T(s) - T(s-1)|| > ε ||T(s)|| & ||E(s) - E(s-1)|| > ε ||E(s)|| do
  • transport iterations
  s = s + 1
  T(s) ⇒ ℒg(s)
  c-1∂tIg + ℒg(s)Ig = qg[T(s)] on Ων ⇒ Ig(s), g ∈ ℕ(nν)
  Ig(s) ⇒ fg(s), Cg±(s), g ∈ ℕ(nν)
  T(s), fg(s), Cg±(s) ⇒ ℳg(s), g ∈ ℕ(nν)
  ∂tYg + ℳg(s)Yg = Qg on Ων & MEB Eq. (28) ⇒ T(s+1), Eg(s+1), Fg(s+1), g ∈ ℕ(nν)

```

**Algorithm 1:** The two-level QD method on the single frequency grid  $\Omega_\nu$ .

### 3.2. The Multilevel QD Method with Two Grids in Frequency

In this section, we review the multilevel QD (MLQD) method that uses two frequency grids to solve the multigroup LOQD equations coupled with the MEB equation [23, 25, 26, 29]. This method introduces the coarse frequency grid

$$\Omega_\nu^* = \{\nu_1 = 0, \nu_2 = \infty\} \quad (29)$$

with one group. The effective grey LOQD equations are formulated on the grid  $\Omega_\nu^*$  for the total radiation energy density

$$E(x, t) = \sum_{g=1}^{n_\nu} E_g(x, t) \quad (30)$$

and total flux

$$F(x, t) = \sum_{g=1}^{n_\nu} F_g(x, t). \quad (31)$$

The effective grey LOQD problem is defined by

$$\frac{\partial E}{\partial t} + \frac{\partial F}{\partial x} + c\bar{\sigma}_E E = c\bar{\sigma}_{BaR} T^4, \quad (32a)$$

$$\frac{1}{c} \frac{\partial F}{\partial t} + c \frac{\partial (\bar{f}E)}{\partial x} + \bar{\sigma}_R F + \bar{\eta} E = 0 \quad (32b)$$

with the boundary conditions

$$F|_{x=0} = (c\bar{C}^-(E - E^+) + F^+)|_{x=0}, \quad F|_{x=X} = (c\bar{C}^+(E - E^-) + F^-)|_{x=X} \quad (33)$$

and the initial conditions

$$E|_{t=0} = E^0, \quad F|_{t=0} = F^0, \quad (34)$$

where

$$E^\pm = \sum_{g=1}^{n_\nu} E_g^\pm, \quad F^\pm = \sum_{g=1}^{n_\nu} F_g^\pm, \quad E^0 = \sum_{g=1}^{n_\nu} E_g^0, \quad F^0 = \sum_{g=1}^{n_\nu} F_g^0, \quad (35)$$

$a_R$  is the Stefan's constant. The grey LOQD equations (32) on the coarse grid  $\Omega_\nu^*$  are derived by summing the group LOQD equations (19) over all groups and formulating exact closures by means of the grey QD factor

$$\bar{f} = \langle f \rangle_E, \quad (36)$$

the grey boundary QD factors

$$\bar{C}^- = \langle C^- \rangle_E|_{x=0}, \quad \bar{C}^+ = \langle C^+ \rangle_E|_{x=X}, \quad (37)$$

the grey opacities

$$\bar{\sigma}_E = \langle \sigma_E \rangle_E, \quad \bar{\sigma}_B = \langle \sigma_B \rangle_B, \quad \bar{\sigma}_R = \langle \sigma_R \rangle_{|F|}, \quad (38)$$

where the notations for the averaged quantities are defined by

$$\langle \psi \rangle_H = \frac{\sum_{g=1}^{n_\nu} \psi_g H_g}{\sum_{g=1}^{n_\nu} H_g}, \quad H_g = \begin{cases} E_g & \text{for } H = E, \\ B_g & \text{for } H = B, \\ |F_g| & \text{for } H = |F|. \end{cases} \quad (39)$$

The compensation term is given by

$$\bar{\eta} = \frac{\sum_{g=1}^{n_\nu} (\sigma_{R,g} - \bar{\sigma}_R) F_g}{\sum_{g=1}^{n_\nu} E_g}. \quad (40)$$

The operator form of Eqs. (32) is the following:

$$\frac{\partial \mathbf{Y}}{\partial t} + \bar{\mathcal{M}} \mathbf{Y} = \mathbf{Q}, \quad \mathbf{Y} = (E, F)^T, \quad (41)$$

where the operator  $\bar{\mathcal{M}} = \bar{\mathcal{M}}[f_g, C_g^\pm, E_g, F_g, T]$  and  $\mathbf{Q} = \mathbf{Q}[T]$ . The effective grey LOQD equations are coupled with the MEB equation in the grey form

$$\frac{\partial \varepsilon(T)}{\partial t} = c(\bar{\sigma}_E E - \bar{\sigma}_B a_R T^4). \quad (42)$$

In summary, the system of equations of the MLQD method on two frequency grids  $\Omega_\nu$  and  $\Omega_\nu^*$  is defined by Eqs. (8), (19), (32), and (42).

Algorithm 2 shows the iterative scheme for the two-grid MLQD method on the  $j$ -th time step. The iterative scheme consists of nested iterations. Here  $\ell$  is the index of inner (low-order) iterations. The outer iteration cycle is the transport iteration. Note that there are no transport sweeps for  $s = 0$ . On each outer iteration, the system of the group LOQD equations on the given grid in frequency  $\Omega_\nu$  and MEB equation is solved by means of the grey LOQD equations. The estimation of temperature is obtained from Eqs. (32) and (42).

$s = -1, T^{(0)} = T^{j-1}, f_g^{(0)} = f_g^{j-1}$   
**while**  $\|T^{(s)} - T^{(s-1)}\| > \epsilon \|T^{(s)}\|$  &  $\|E^{(s)} - E^{(s-1)}\| > \epsilon \|E^{(s)}\|$  **do**  
    • transport (outer) iterations  
     $s = s + 1$   
    **if**  $s > 0$  **then**  
         $T^{(s)} \Rightarrow \mathcal{L}_g^{(s)}$   
         $c^{-1} \partial_t I_g + \mathcal{L}_g^{(s)} I_g = q_g[T^{(s)}]$  on  $\Omega_\nu \Rightarrow I_g^{(s)}, g \in \mathbb{N}(n_\nu)$   
         $I_g^{(s)} \Rightarrow f_g^{(s)}, C_g^{\pm(s)}, g \in \mathbb{N}(n_\nu)$   
     $\ell = -1, T^{(1,s)} = T^{(s)}$   
    **while**  $\|T^{(\ell,s)} - T^{(\ell-1,s)}\| > \tilde{\epsilon} \|T^{(\ell,s)}\|$  &  $\|E^{(\ell,s)} - E^{(\ell-1,s)}\| > \tilde{\epsilon} \|E^{(\ell,s)}\|$  **do**  
         $\ell = \ell + 1$   
         $T^{(\ell,s)}, f_g^{(s)}, C_g^{\pm(s)} \Rightarrow \mathcal{M}_g^{(\ell,s)}$   
         $\partial_t \mathbf{Y}_g + \mathcal{M}_g^{(\ell,s)} \mathbf{Y}_g = \mathbf{Q}_g[T^{(\ell,s)}]$  on  $\Omega_\nu \Rightarrow E_g^{(\ell,s)}, F_g^{(\ell,s)}, g \in \mathbb{N}(n_\nu)$   
         $T^{(\ell,s)}, E_g^{(\ell,s)}, F_g^{(\ell,s)}, f_g^{(s)}, C_g^{\pm(s)} \Rightarrow \bar{\mathcal{M}}^{(\ell,s)}$   
         $\partial_t \mathbf{Y} + \bar{\mathcal{M}}^{(\ell,s)} \mathbf{Y} = \mathbf{Q}$  on  $\Omega_\nu^*$  & MEB Eq. (42)  $\Rightarrow T^{(\ell+1,s)}, E^{(\ell+1,s)}, F^{(\ell+1,s)}$   
     $T^{(s+1)} \leftarrow T^{(\ell+1,s)}$

**Algorithm 2:** The MLQD method with two frequency grids  $\Omega_\nu$  and  $\Omega_\nu^*$ .

#### 4. The Multilevel QD Method with Multigrid in Frequency

We now define a sequence of nested grids in frequency

$$\mathcal{G}_\Omega^\Gamma = \{\Omega_\nu^\gamma, \gamma \in \mathbb{N}(\Gamma)\}, \quad \Omega_\nu^\gamma = \{\nu_p^\gamma, p \in \mathbb{N}(n_\nu^\gamma + 1)\}, \quad \Omega_\nu^1 \equiv \Omega_\nu, \quad \Omega_\nu^\Gamma \equiv \Omega_\nu^*, \quad (43)$$

where  $\gamma$  is the grid index, and  $p$  is the index of the frequency interval  $\omega_p^\gamma = [\nu_p^\gamma, \nu_{p+1}^\gamma]$ . These grids are defined by successive coarsening. The  $p$ -th interval of the grid  $\Omega_\nu^\gamma$  is formed by intervals of the grid  $\Omega_\nu^{\gamma-1}$  with the set of indices  $\Lambda_p^\gamma = \{p' : \omega_{p'}^{\gamma-1} \in \omega_p^\gamma\}$  and hence  $\omega_p^\gamma = \bigcup_{p' \in \Lambda_p^\gamma} \omega_{p'}^{\gamma-1} = \bigcup_{g \in \tilde{\Lambda}_p^\gamma} \omega_g^1$ ,

where  $\tilde{\Lambda}_p^\gamma = \{g : \omega_g^1 \in \omega_p^\gamma\}$ . The group LOQD equations on the coarse grid  $\Omega_\nu^\gamma$  for

$$E_p^\gamma = \int_{\nu_p^\gamma}^{\nu_{p+1}^\gamma} E_\nu d\nu, \quad F_p^\gamma = \int_{\nu_p^\gamma}^{\nu_{p+1}^\gamma} F_\nu d\nu \quad (44)$$

are derived by projecting the group LOQD equations from the fine grid  $\Omega_\nu^1$  to  $\Omega_\nu^\gamma$  and applying exact closures to formulate the equations for the unknowns on  $\Omega_\nu^\gamma$ . The LOQD equations on the coarse grid  $\Omega_\nu^\gamma$  are given by

$$\frac{\partial E_p^\gamma}{\partial t} + \frac{\partial F_p^\gamma}{\partial x} + c \bar{\sigma}_{E,p}^\gamma E_p^\gamma = 2 \bar{\sigma}_{B,p}^\gamma B_p^\gamma, \quad (45a)$$

$$\frac{1}{c} \frac{\partial F_p^\gamma}{\partial t} + c \frac{\partial (\bar{f}_p^\gamma E_p^\gamma)}{\partial x} + \bar{\sigma}_{R,p}^\gamma F_p^\gamma + \bar{\eta}_p^\gamma E_p^\gamma = 0 \quad (45b)$$

with the boundary conditions

$$F_p^\gamma|_{x=0} = (c \bar{C}_p^{\gamma-} (E_p^\gamma - E_p^{\gamma, in+}) + F_p^{\gamma, in+})|_{x=0}, \quad (46a)$$



$$F_p^\gamma|_{x=X} = (c\bar{C}_p^{\gamma+}(E_p^\gamma - E_p^{\gamma,in-}) + F_p^{\gamma,in-})|_{x=X} \quad (46b)$$

and the initial conditions

$$E_p^\gamma|_{t=0} = E_p^{\gamma,0}, \quad F_p^\gamma|_{t=0} = F_p^{\gamma,0}. \quad (47)$$

Hereafter the equations (45) are referred to as coarse-group equations. The coefficients of Eqs. (45) are averaged with the solution on  $\Omega_\nu^\gamma$  and defined as follows:

$$\bar{f}_p^\gamma = \langle f \rangle_{E,p}^\gamma, \quad \bar{C}_p^{\gamma\pm} = \langle C^\pm \rangle_{E,p}^\gamma, \quad \bar{\sigma}_{E,p}^\gamma = \langle \sigma_E \rangle_{E,p}^\gamma, \quad \bar{\sigma}_{B,p}^\gamma = \langle \sigma_B \rangle_{B,p}^\gamma, \quad \bar{\sigma}_{R,p}^\gamma = \langle \sigma_R \rangle_{|F|,p}^\gamma, \quad (48)$$

where the notations for the averaged functions are given by

$$\langle \psi \rangle_{H,p}^\gamma = \frac{\sum_{g \in \tilde{\Lambda}_p^\gamma} \psi_g^1 H_g^1}{\sum_{g \in \tilde{\Lambda}_p^\gamma} H_g^1}, \quad H_g^1 = \begin{cases} E_g^1 & \text{for } H = E, \\ B_g^1 & \text{for } H = B, \\ |F_g^1| & \text{for } H = |F|. \end{cases} \quad (49)$$

The compensation term in the first moment equation (45b) is defined by

$$\bar{\eta}_p^\gamma = \frac{\sum_{g \in \tilde{\Lambda}_p^\gamma} (\sigma_{R,g}^1 - \bar{\sigma}_{R,p}^\gamma) F_g^1}{\sum_{g \in \tilde{\Lambda}_p^\gamma} E_g^1}. \quad (50)$$

The operator form of the LOQD equations on the grid  $\Omega_\nu^\gamma$  is given by

$$\frac{\partial \mathbf{Y}_p^\gamma}{\partial t} + \mathcal{M}_p^\gamma \mathbf{Y}_p^\gamma = \mathbf{Q}_p^\gamma, \quad \mathbf{Y}_p^\gamma = (E_p^\gamma, F_p^\gamma)^T, \quad p \in \mathbb{N}(n_\nu^\gamma). \quad (51)$$

The solution on the grid  $\Omega_\nu^\gamma$  is used to form the grey LOQD equations on the grid  $\Omega_\nu^\Gamma$  that are defined by

$$\frac{\partial \mathbf{Y}_1^\Gamma}{\partial t} + \mathcal{M}_1^\Gamma \mathbf{Y}_1^\Gamma = \mathbf{Q}_1^\Gamma, \quad \mathbf{Y}_1^\Gamma = (E_1^\Gamma, F_1^\Gamma)^T. \quad (52)$$

The coefficients of Eq. (52) are given by

$$\bar{f}_1^\Gamma = \langle f \rangle_E^{\gamma \rightarrow \Gamma}, \quad \bar{C}_1^{\Gamma\pm} = \langle C^\pm \rangle_E^{\gamma \rightarrow \Gamma}, \quad \bar{\sigma}_{E,1}^\Gamma = \langle \sigma_E \rangle_E^{\gamma \rightarrow \Gamma}, \quad \bar{\sigma}_{B,1}^\Gamma = \langle \sigma_B \rangle_B^{\gamma \rightarrow \Gamma}, \quad \bar{\sigma}_{R,1}^\Gamma = \langle \sigma_R \rangle_{|F|}^{\gamma \rightarrow \Gamma}, \quad (53)$$

$$\bar{\eta}_1^\Gamma = \frac{\sum_{p=1}^{n_\nu^\gamma} (\bar{\sigma}_{R,p}^\gamma - \bar{\sigma}_{R,1}^\Gamma) F_p^\gamma}{\sum_{p=1}^{n_\nu^\gamma} E_p^\gamma}, \quad (54)$$

where

$$\langle \psi \rangle_H^{\gamma \rightarrow \Gamma} = \frac{\sum_{p=1}^{n_\nu^\gamma} \bar{\psi}_p^\gamma H_p^\gamma}{\sum_{p=1}^{n_\nu^\gamma} H_p^\gamma}, \quad H_p^\gamma = \begin{cases} E_p^\gamma & \text{for } H = E, \\ B_p^\gamma & \text{for } H = B, \\ |F_p^\gamma| & \text{for } H = |F|. \end{cases} \quad (55)$$

The MEB equation coupled with the LOQD equations on the coarsest grid  $\Omega_\nu^\Gamma$  has the following form:

$$\frac{\partial \varepsilon(T)}{\partial t} = c(\bar{\sigma}_{E,1}^\Gamma E_1^\Gamma - \bar{\sigma}_{B,1}^\Gamma a_R T^4). \quad (56)$$

The MLQD method for TRT problems on the sequence of grids in photon frequency  $\mathcal{G}_\Omega^\Gamma$  is defined by Eqs. (8), (19), (45), (52), and (56).

To solve the hierarchy of LOQD equations coupled with the MEB equation, we apply  $W$  and full ( $F$ ) multigrid cycles to visit grids [35]. Algorithm 3 describes the MLQD method on the hierarchy of frequency grids  $\mathcal{G}_\Omega^\Gamma$ . The set  $\mathcal{S} = \{\gamma_k, k \in \mathbb{N}(K)\}$  defines the schedule of visiting grids after each evaluation of temperature on the coarsest grid  $\Omega_\nu^\Gamma$ . Figure 1a shows the diagram of the  $W$ -cycle for three grids ( $\Gamma = 3$ ) for which  $\mathcal{S} = \{2\}$  and  $K = 1$ . The  $F$ -cycle on four grids ( $\Gamma = 4$ ) with  $K = 2$  and the schedule  $\mathcal{S} = \{3, 2\}$  is illustrated in Fig. 1b. The MLQD method with two grids (Sec. 3.2) is equivalent to Algorithm 3 with the  $V$ -cycle the diagram of which is shown in Fig. 1c. The cycles are executed until either the convenience criteria for  $T$  and  $E$  are satisfied or the number of cycles reaches the given maximum number  $\ell_{max}$ .

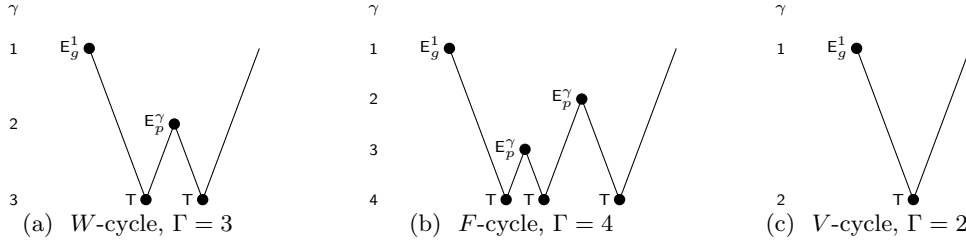


Figure 1: Diagrams of multigrid cycles on hierarchies of  $\Gamma$  grids in frequency.  $E_g^1$  - calculation of spectrum on the fine grid  $\Omega_\nu^1$  by solving the multigroup LOQD equations,  $T$  - calculation of temperature by solving coupled grey LOQD and MEB equations on  $\Omega_\nu^\Gamma$ ,  $E_p^\gamma$  - calculation of spectrum on  $\Omega_\nu^\gamma$  ( $\gamma > 1$ ) by solving the coarse-group LOQD equations.

The multigrid cycle starts from calculating the spectrum on the fine grid  $\Omega_\nu^1$  for the current estimation of temperature. The new temperature is evaluated by solving the effective grey problem on  $\Omega_\nu^\Gamma$  formulated with the fine-grid spectrum. Then the spectrum is computed on some coarse grid  $\Omega_\nu^\gamma$  for  $1 < \gamma < \Gamma$  using the new temperature. On the next stage, the obtained coarse-grid spectrum on  $\Omega_\nu^\gamma$  is used to average opacities and factors and calculate their grey quantities. This forms the updated effective grey problem on  $\Omega_\nu^\Gamma$  that is solved to get the temperature at this stage of the cycle. Then these two elements of the cycle are repeated using the coarse grid according to the schedule  $\mathcal{S}$ .

The coarse-group LOQD equations on  $\Omega_\nu^\gamma$  are derived by exact averaging the LOQD equations on  $\Omega_\nu^{\gamma-1}$ . As a results, if the group LOQD equations on these grids are defined with the same  $T$ , then

$$E_p^\gamma = \sum_{p' \in \Lambda_p^\gamma} E_{p'}^{\gamma-1} = \sum_{g \in \tilde{\Lambda}_p^\gamma} E_g^1, \quad F_p^\gamma = \sum_{p' \in \Lambda_p^\gamma} F_{p'}^{\gamma-1} = \sum_{g \in \tilde{\Lambda}_p^\gamma} F_g^1. \quad (57)$$

Thus, there is no change in spectrum from grid to grid in this case. The multigrid cycles are defined in such a way that a grid is visited only after the temperature update was performed on the coarsest grid  $\Omega_\nu^\Gamma$ . If the spectrum is evaluated on  $\Omega_\nu^{\gamma'}$  with the current estimate of temperature then all coarser grids with  $\gamma' < \gamma < \Gamma$  are skipped on the way down to  $\Omega_\nu^\Gamma$ . After evaluation

of temperature on  $\Omega_\nu^\Gamma$  the algorithm is scheduled to update the spectrum on the grid  $\Omega_\nu^{\gamma''}$ . The algorithm skips all grids with  $\gamma'' < \gamma < \Gamma$  on the way up to the scheduled finer grid.

```

 $s = -1, T^{(0)} = T^{j-1}, f_g^{(0)} = f_g^{j-1}$ 
while  $\|T^{(s)} - T^{(s-1)}\| > \epsilon \|T^{(s)}\| \ \&\ \ \|E^{(s)} - E^{(s-1)}\| > \epsilon \|E^{(s)}\|$  do
  • transport (outer) iterations
   $s = s + 1$ 
  if  $s > 0$  then
     $T^{(s)} \Rightarrow \mathcal{L}_g^{(s)}$ 
     $c^{-1} \partial_t I_g + \mathcal{L}_g^{(s)} I_g = q_g[T^{(s)}]$  on  $\Omega_\nu^1 \Rightarrow I_g^{(s)}, g \in \mathbb{N}(n_\nu^1)$ 
     $I_g^{(s)} \Rightarrow f_g^{(s)}, C_g^{\pm(s)}, g \in \mathbb{N}(n_\nu^1)$ 
   $\ell = -1, T^{(1,s)} = T^{(s)}$ 
  while  $\ell \leq \ell_{max}$  or  $\|T^{(\ell,s)} - T^{(\ell-1,s)}\| > \tilde{\epsilon} \|T^{(\ell,s)}\| \ \&\ \ \|E^{(\ell,s)} - E^{(\ell-1,s)}\| > \tilde{\epsilon} \|E^{(\ell,s)}\|$  do
    • low-order (inner) iterations
     $\ell = \ell + 1$ 
    calculation of fine-grid spectrum on  $\Omega_\nu^1$ 
     $T^{(\ell,s)}, f_g^{(s)}, C_g^{\pm(s)} \Rightarrow \mathcal{M}_g^{1(\ell,s)}$ 
     $\partial_t \mathbf{Y}_g^1 + \mathcal{M}_g^{1(\ell,s)} \mathbf{Y}_g^1 = \mathbf{Q}_g^1[T^{(\ell,s)}]$  on  $\Omega_\nu^1 \Rightarrow E_g^{1(\ell,s)}, F_g^{1(\ell,s)}, g \in \mathbb{N}(n_\nu^1)$ 
     $\tilde{T}^{[1]} = T^{(\ell,s)}$ 
    for  $k \leftarrow 0$  to  $K$  do
       $\gamma \leftarrow 1$ 
      if  $k > 0$  then
         $\gamma \leftarrow \gamma_k \in \mathcal{S}$ 
        calculation of coarse-grid spectrum on  $\Omega_\nu^\gamma$ 
         $\tilde{T}^{[k]}, E_g^{1(\ell,s)}, F_g^{1(\ell,s)}, f_g^{(s)}, C_g^{\pm(s)} \Rightarrow \mathcal{M}_p^{\gamma[k]}$ 
         $\partial_t \mathbf{Y}_p^\gamma + \mathcal{M}_p^{\gamma[k]} \mathbf{Y}_p^\gamma = \mathbf{Q}_p^\gamma[\tilde{T}^{[k]}]$  on  $\Omega_\nu^\gamma \Rightarrow E_p^{\gamma[k]}, F_p^{\gamma[k]}, p \in \mathbb{N}(n_\nu^\gamma)$ 
         $\tilde{T}^{[k]}, E_p^{\gamma[k]}, F_p^{\gamma[k]} \Rightarrow \mathcal{M}_1^{\Gamma[k]}$ 
         $\partial_t \mathbf{Y}_1^\Gamma + \mathcal{M}_1^{\Gamma[k]} \mathbf{Y}_1^\Gamma = \mathbf{Q}_1^\Gamma$  on  $\Omega_\nu^\Gamma$  & MEB Eq. (56)  $\Rightarrow \tilde{T}^{[k+1]}, E_1^\Gamma, F_1^\Gamma$ 
       $T^{(\ell+1,s)} \leftarrow \tilde{T}^{[k+1]}$ 
     $T^{(s+1)} \leftarrow T^{(\ell+1,s)}$ 

```

**Algorithm 3:** The MLQD method with multiple grids in frequency  $\Omega_\nu^\gamma$ ,  $\gamma \in \mathbb{N}(\Gamma)$ .

## 5. Discretization of Equations

The system of the high-order RT, LOQD, and MEB equations is approximated by the implicit Euler time integration scheme. The opacities and emission terms are evaluated at the current time level. Thus, the implicitly balanced time integration scheme is applied [36]. The RT equation is approximated in space with the simple corner balance method [37]. The second-order finite volume method is applied to discretize the multigroup LOQD equations on  $\Omega_\nu^1$  over space [29]. We define the spatial mesh  $\{x_{i-1/2}, i \in \mathbb{N}(n_x + 1), x_{1/2} = 0, x_{n_x+1/2} = X\}$ . The photon balance equation

(19a) is integrated over the  $i$ -th cell ( $x_{i-1/2} \leq x \leq x_{i+1/2}$ ). The first moment equation (19b) is integrated over  $x_{i-1} \leq x \leq x_i$ , where  $x_i = \frac{1}{2}(x_{i-1/2} + x_{i+1/2})$ . The discretized LOQD equations (19) on  $\Omega_\nu^1$  at  $t = t^j$  have the following form:

$$\frac{\Delta x_i}{\Delta t^j} \left( E_{g,i}^{1,j} - E_{g,i}^{1,j-1} \right) + F_{g,i+1/2}^{1,j} - F_{g,i-1/2}^{1,j} + c \sigma_{E,g,i}^{1,j} \Delta x_j E_{g,i}^{1,j} = \sigma_{B,g,i}^{1,j} \Delta x_i B_{g,i}^{1,j}, \quad (58a)$$

$$\frac{\Delta x_{i+1/2}}{c \Delta t^j} \left( F_{g,i+1/2}^{1,j} - F_{g,i+1/2}^{1,j-1} \right) + c \left( f_{g,i+1}^{1,j} E_{g,i+1}^{1,j} - f_{g,i}^{1,j} E_{g,i}^{1,j} \right) + \sigma_{R,g,i+1/2}^{1,j} \Delta x_{i+1/2} F_{g,i+1/2}^{1,j} = 0, \quad (58b)$$

where

$$\Delta x_i = x_{i+1/2} - x_{i-1/2}, \quad (59)$$

$$\sigma_{R,g,i+1/2}^{1,j} = \frac{\sigma_{R,g,i}^{1,j} \Delta x_i + \sigma_{R,g,i+1}^{1,j} \Delta x_{i+1}}{\Delta x_i + \Delta x_{i+1}}. \quad (60)$$

$j$  is the index of the time step. Integer  $\pm \frac{1}{2}$  subscripts refer to cell-edge quantities, and integer subscripts refer to cell-average quantities.

The spatial approximation of the coarse-group LOQD equations on  $\Omega_\nu^\gamma$  is algebraically consistent with the group LOQD equations on the fine grid  $\Omega_\nu^1$ . The discretized LOQD equations on  $\Omega_\nu^\gamma$  are given by

$$\frac{\Delta x_i}{\Delta t^j} \left( E_{p,i}^{\gamma,j} - E_{p,i}^{\gamma,j-1} \right) + F_{p,i+1/2}^{\gamma,j} - F_{p,i-1/2}^{\gamma,j} + c \bar{\sigma}_{E,p,i}^{\gamma,j} \Delta x_j E_{p,i}^{\gamma,j} = \bar{\sigma}_{B,p,i}^{\gamma,j} \Delta x_i B_{p,i}^{\gamma,j}, \quad (61a)$$

$$\frac{\Delta x_{i+1/2}}{c \Delta t^j} \left( F_{p,i+1/2}^{\gamma,j} - F_{p,i+1/2}^{\gamma,j-1} \right) + c \left( (\bar{f}_{p,i+1}^{\gamma,j} + \hat{\eta}_{p,i+1/2}^{\gamma,j}) E_{p,i+1}^{\gamma,j} - (\bar{f}_{p,i}^{\gamma,j} + \hat{\eta}_{p,i+1/2}^{\gamma,j}) E_{p,i}^{\gamma,j} \right) + \bar{\sigma}_{R,p,i+1/2}^{\gamma,j} \Delta x_{i+1/2} F_{p,i+1/2}^{\gamma,j} = 0, \quad (61b)$$

where

$$\bar{f}_{p,i}^{\gamma,j} = \langle f_i^j \rangle_{E,p}^\gamma, \quad \bar{\sigma}_{E,p,i}^{\gamma,j} = \langle \sigma_{E,i}^j \rangle_{E,p}^\gamma, \quad \bar{\sigma}_{B,p,i}^{\gamma,j} = \langle \sigma_{B,i}^j \rangle_{B,p}^\gamma, \quad \bar{\sigma}_{R,p,i+1/2}^{\gamma,j} = \langle \sigma_{R,i+1/2}^j \rangle_{|F|,p}^\gamma, \quad (62)$$

$$\langle \psi_\alpha^j \rangle_{H,p}^\gamma = \frac{\sum_{g \in \tilde{\Lambda}_p^\gamma} \psi_{g,\alpha}^{1,j} H_{g,\alpha}^{1,j}}{\sum_{g \in \tilde{\Lambda}_p^\gamma} H_{g,\alpha}^{1,j}}, \quad H_{g,\alpha}^{1,j} = \begin{cases} E_{g,i}^{1,j}, & \alpha = i \text{ for } H = E, \\ B_{g,i}^{1,j}, & \alpha = i \text{ for } H = B, \\ |F_{g,i+1/2}^{1,j}|, & \alpha = i + \frac{1}{2} \text{ for } H = |F|. \end{cases} \quad (63)$$

$$\hat{\eta}_{p,i+1/2}^{\gamma,j} = \begin{cases} c \frac{\xi_{p,i+1/2}^{\gamma,j}}{\sum_{g \in \tilde{\Lambda}_p^\gamma} E_{g,i+1}^{1,j}} & \text{for } \xi_{p,i+1/2}^{\gamma,j} > 0, \\ 0 & \text{for } \xi_{p,i+1/2}^{\gamma,j} \leq 0, \end{cases} \quad \tilde{\eta}_{p,i+1/2}^{\gamma,j} = \begin{cases} 0 & \text{for } \xi_{p,i+1/2}^{\gamma,j} \geq 0, \\ -c \frac{\xi_{p,i+1/2}^{\gamma,j}}{\sum_{g \in \tilde{\Lambda}_p^\gamma} E_{g,i}^{1,j}} & \text{for } \xi_{p,i+1/2}^{\gamma,j} < 0, \end{cases} \quad (64)$$

$$\xi_{p,i+1/2}^{\gamma,j} = \sum_{g \in \tilde{\Lambda}_p^\gamma} \left( \sigma_{R,g,i+1/2}^{1,j} - \bar{\sigma}_{R,p,i+1/2}^{\gamma,j} \right) F_{g,i+1/2}^{1,j}. \quad (65)$$

Similarly, the discretized LOQD equations on the grid  $\Omega_\nu^\gamma$  (Eqs. (61)) are averaged over groups to derive the discrete grey LOQD equations (Eqs. (52)) on the grid  $\Omega_\nu^\Gamma$  and define their coefficients (53). The discretized MEB equations has the form:

$$\frac{\partial \varepsilon(T_i^j)}{\partial t} = c \left( \bar{\sigma}_{E,1,i}^{\Gamma,j} E_{1,i}^{\Gamma,j} - \bar{\sigma}_{B,1,i}^{\Gamma,j} a_R(T_i^j)^4 \right). \quad (66)$$

The grey LOQD equations on  $\Omega_\nu^\Gamma$  and the MEB equation (Eq. (66)) are solved by Newton's method. The grey opacity

$$\bar{\sigma}_{E,1}^\Gamma(T) = \frac{\sum_{p=1}^{n_\nu^\gamma} \bar{\sigma}_{E,p}^\gamma(T) E_p^\gamma(T)}{\sum_{p=1}^{n_\nu^\gamma} E_p^\gamma(T)}, \quad \gamma \in \mathcal{S} \quad (67)$$

depends locally on  $T$  through  $\sigma_{E,g}(T)$  on  $\Omega_\nu^1$  and globally through the coarse-grid  $E_p^\gamma(T)$  as well as  $E_g^1(T)$  applied to compute the opacity  $\bar{\sigma}_{E,p}^\gamma$  on  $\Omega_\nu^\gamma$ . The Fréchet derivative of  $\bar{\sigma}_{E,1}^\Gamma$  is used in the linearized equations to account for its variation due to change in temperature. The Fréchet derivative  $\mathcal{D}\bar{\sigma}_{E,1}^\Gamma$  is a linear operator such that

$$\bar{\sigma}_{E,1}^\Gamma(T + \Delta T) - \bar{\sigma}_{E,1}^\Gamma(T) = \mathcal{D}\bar{\sigma}_{E,1}^\Gamma \Delta T + \rho(T, \Delta T), \quad (68)$$

where

$$\frac{\rho(T, \Delta T)}{\|\Delta T\|} \rightarrow 0 \quad \text{as} \quad \|\Delta T\| \rightarrow 0. \quad (69)$$

In discrete space,  $\mathcal{D}\bar{\sigma}_{E,1}^\Gamma$  is a matrix. There are different ways to estimate  $\mathcal{D}\bar{\sigma}_{E,1}^\Gamma$ . A robust and efficient variant is to approximate it by the diagonal matrix given by [25, 26]

$$\mathcal{D}\bar{\sigma}_{E,1}^\Gamma = \text{diag} \left[ (D\bar{\sigma}_{E,1}^\Gamma)_1^{[k]}, \dots, (D\bar{\sigma}_{E,1}^\Gamma)_i^{[k]}, \dots, (D\bar{\sigma}_{E,1}^\Gamma)_{n_x}^{[k]} \right], \quad (70)$$

where

$$(D\bar{\sigma}_{E,1}^\Gamma)_i^{[k]} = \frac{\bar{\sigma}_{E,1,i}^\Gamma(\tilde{T}^{[k]}) - \bar{\sigma}_{E,1,i}^\Gamma(\tilde{T}^{[k-1]})}{\tilde{T}_i^{[k]} - \tilde{T}_i^{[k-1]}}. \quad (71)$$

The value of the discrete Fréchet derivative (70) is fixed during Newton's iterations for solving of the linearized grey LOQD and MEB equations.

## 6. Numerical Results

In this section, numerical results of the Fleck-Cummings (FC) test are presented [7]. The test is defined for a slab ( $0 \leq x \leq 4$  cm) with one material. The spectral opacity of the material is given by

$$\sigma_\nu(T) = \frac{27}{(h\nu)^3} (1 - e^{-\frac{h\nu}{kT}}). \quad (72)$$

There is incoming radiation with the black-body spectrum at  $kT_b=1$  keV at the left boundary. The right boundary is vacuum. The initial temperature in the domain is  $kT_0=10^{-3}$  keV.

$I_g|_{t=0} = B_g(T_0)$ . The material energy is given by  $\varepsilon(T) = c_v T$  with  $c_v = 0.5917 a_R T_b^3$ . The spatial mesh is uniform with 10 intervals. The time interval of the problem is  $t \in [0, 3 \text{ ns}]$ . The frequency grid  $\Omega_\nu$  is defined by  $n_\nu = 256$  groups over the range  $0 \leq h\nu \leq 10^7$  keV. There are  $n_\nu - 2$  groups evenly spaced in logarithmic scale between  $h\nu_a = 10^{-4}$  keV and  $h\nu_b = 10$  keV. The double  $S_8$  Gauss-Legendre quadrature set is used and hence there are 16 angular directions. The test is calculated with two time steps:  $\Delta t = 2 \times 10^{-2}$  ns and  $\Delta t = 4 \times 10^{-2}$  ns. The parameters of convergence criteria are  $\epsilon = 10^{-6}$  and  $\tilde{\epsilon} = 10^{-7}$ . Figure 2 shows temperature and total energy density at various instants of time obtained with  $\Delta t = 2 \times 10^{-2}$  ns and illustrates evolution of heat and radiation waves.

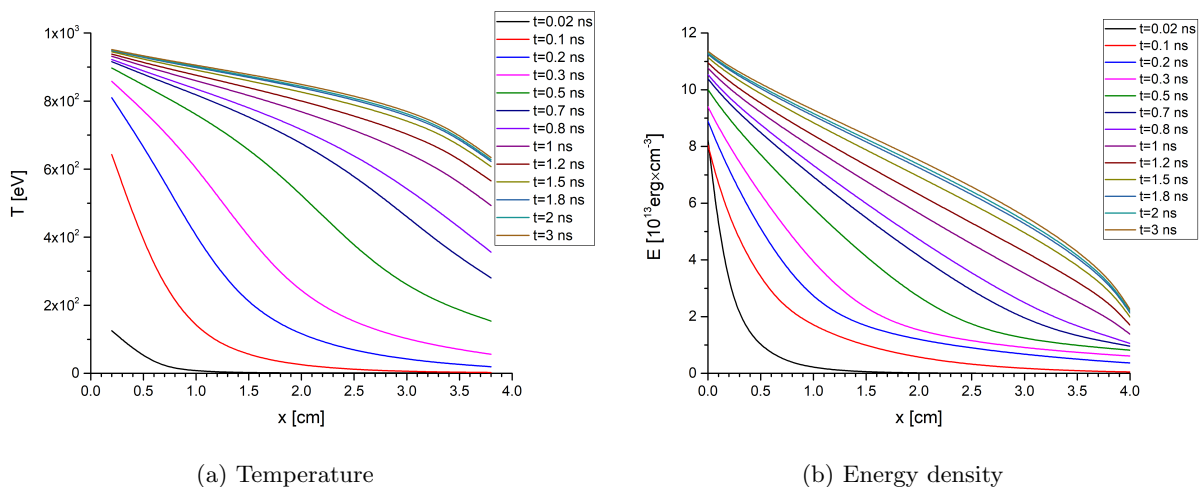


Figure 2: Numerical solution of the FC test with 256 groups and  $\Delta t = 2 \times 10^{-2}$  ns.

The algorithms with  $W$  and  $F$  cycles (see Fig. 1) were studied on a variety of grid hierarchies with different  $\Gamma$ . The grids are formed by successive and uniform coarsening. They are defined by the number of groups, i.e.  $n_\nu$ . The number of Newton's iterations for solving the grey LOQD and MEB equations to evaluate temperature is equal to 1. The algorithms use different values of the parameter  $\ell_{max}$  that restricts the number of inner (low-order) iterations and hence the number of multigrid cycles on each transport iteration.

Figures 3 and 4 present the results of the algorithms on selected hierarchies of grids in tests with  $\Delta t = 2 \times 10^{-2}$  ns and  $\Delta t = 4 \times 10^{-2}$  ns, respectively. These figures show the numbers of transport iterations ( $M_{ti}$ ), cycles ( $M_c$ ), and low-order solves ( $M_{lo}$ ) versus time instant for each algorithm in two test cases. For each value of  $\Gamma$ , the results are presented for such combination of the type of algorithm,  $\ell_{max}$  and set of grids that yields the smallest total number of transport iterations and total number of cycles. The hierarchies of grids and the value of  $\ell_{max}$  are indicated in the figures. Tables 1 and 2 show the total numbers of transport iterations ( $N_{ti}$ ), cycles ( $N_c$ ), low-order solves ( $N_{lo}$ ) in tests with  $\Delta t = 2 \times 10^{-2}$  ns and  $\Delta t = 4 \times 10^{-2}$  ns, respectively.

Each time step is a different case for iteration algorithms. However, there are similarities between instants over characteristic stages of the TRT problem, such as (a) initial radiation penetration in the domain, (b) radiation wave formation, (c) well-developed wave, and (d) approaching steady-state regime. The differences in evolution of the solution during these stages affect the

numbers of iterations and cycles. These effects can be seen in Figures 3 and 4. The bigger the time step the larger the change in the solution over the time interval. This leads to some increase in numbers of iterations.

The obtained results show that the algorithms with multiple grids in frequency significantly reduce the number of cycles. We note that each algorithm has different computational costs. They depend on (i) the number of transport iterations and (ii) the number of low-order solves, i.e. the number of times the group-wise LOQD equations are solved. Tables 1 and 2 also show the ratio between the number of low-order solves required in the tests by the algorithm ( $N_{lo}$ ) and this number in the case of the  $V$ -cycle ( $\Gamma = 2$ ).

The number of transport iterations ( $N_{ti}$ ) is an important factor of algorithm efficiency, because their computational costs are directly proportional to the number of angular directions and as well as number of frequency groups in the problem. There is a small variation in  $N_{ti}$  among the presented algorithms. In the test with  $\Delta t = 2 \times 10^{-2}$  ns, the algorithm with the  $V$ -cycle on 2 grids needs 365 transport iterations. This can be considered as a target value of  $N_{ti}$  in this test. Most of the algorithms execute 366-367 transport iterations. The algorithm with the  $W$ -cycle and  $\ell_{max} = 2$  on the grids with  $n_{\nu}^{\gamma} = 256, 32, 1$  requires 362 transport iterations. The algorithm with the  $F$ -cycle on 7 grids with  $N_{ti} = 366$  executes the smallest number of low-order solves. In the case of  $\Delta t = 4 \times 10^{-2}$  ns, the algorithm with the  $V$ -cycle executes 210 transport iterations. Almost all multigrid algorithms require 209 transport iterations in this case. Among them the algorithm with the  $F$ -cycle on 6 grids has the smallest number of low-order solves. The algorithm with the  $F$ -cycle on the grids with  $\Gamma = 5$  executes even less number of low-order solves  $N_{lo}$ , but needs 2 more transport iterations.

To demonstrate convergence behavior of different algorithms, we use one of initial instants, namely,  $t = 8 \times 10^{-2}$  ns. The evolution of both temperature and radiation waves is fast at this early stage. Figure 5 presents convergence of temperature with transport iterations ( $\|\Delta T^{(s)}\|_{\infty}$ ) in the case of  $\Delta t = 2 \times 10^{-2}$  ns and  $\Delta t = 4 \times 10^{-2}$  ns. The algorithms converge rapidly with slightly different rates requiring the same number of transport iterations. Figure 6 shows iterative convergence of temperature over cycles ( $\|\Delta \tilde{T}^{[k]}\|_{\infty}$ ) versus number of low-order solves. The patterns of convergence of inner (low-order) iterations are different. At this instant of time, the most efficient algorithms are (i) the  $F$ -cycle with  $\ell_{max} = 1$  on 7 grids for  $\Delta t = 2 \times 10^{-2}$  ns, and (ii) the  $F$ -cycle with  $\ell_{max} = 3$  on 5 grids for  $\Delta t = 4 \times 10^{-2}$  ns. They require the smallest number of low-order solves. We note that it takes more cycles and low-order solves in the case of the larger time step. The number of transport iterations is the same for both time steps. Thus, the computational effort is shifted to the projected subspace for  $\Delta t = 4 \times 10^{-2}$  ns at this instant.

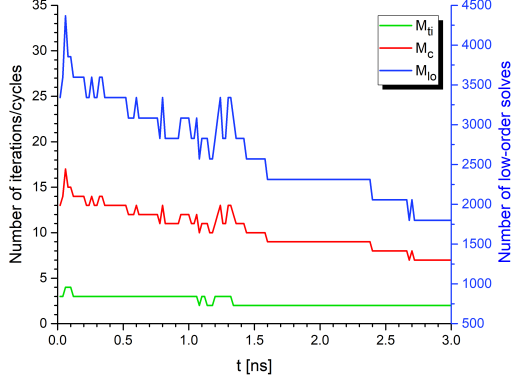
Table 1: Performance of algorithms in the FC test with 256 groups and  $\Delta t = 2 \times 10^{-2}$  ns over 150 time steps for  $t \in [0, 3 \text{ ns}]$

Cycle	$\Gamma$	$n_{\nu}^{\gamma}, \gamma \in \mathbb{N}(\Gamma)$	$\ell_{max}$	$N_{ti}$	$N_c$	$N_{lo}$	$\frac{N_{lo}}{N_{lo}(V, \ell_{max}=4)}$
<i>V</i>	2	256, 1	4	365	1547	397579	1
<i>W</i>	3	256, 32, 1	2	362	901	261290	0.66
<i>F</i>	4	256, 32, 16, 1	2	366	897	275379	0.69
<i>F</i>	5	256, 32, 16, 4, 1	2	366	896	279552	0.70
<i>F</i>	6	256, 128, 64, 32, 16, 1	1	367	517	259017	0.65
<i>F</i>	7	256, 128, 32, 16, 8, 4, 1	1	366	516	232200	0.58

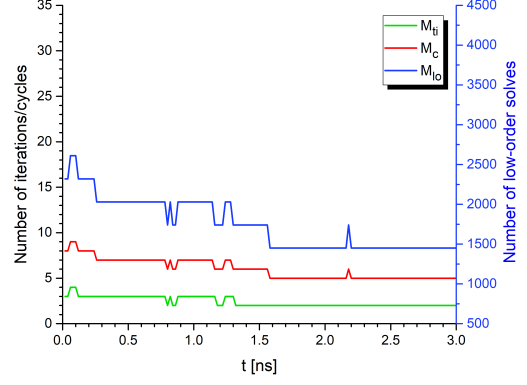
Table 2: Performance of algorithms in the FC test with 256 groups and  $\Delta t = 4 \times 10^{-2}$  ns over 75 time steps for  $t \in [0, 3 \text{ ns}]$

Cycle	$\Gamma$	$n_{\nu}^{\gamma}, \gamma \in \mathbb{N}(\Gamma)$	$\ell_{max}$	$N_{ti}$	$N_c$	$N_{lo}$	$\frac{N_{lo}}{N_{lo}(V, \ell_{max}=6)}$
<i>V</i>	2	256, 1	6	210	1262	324334	1
<i>W</i>	3	256, 32, 1	3	209	722	209380	0.65
<i>F</i>	4	256, 32, 16, 1	3	209	695	213365	0.66
<i>F</i>	5	256, 32, 16, 4, 1	2	211	519	178536	0.55
<i>F</i>	6	256, 64, 32, 16, 4, 1	2	209	516	194532	0.60
<i>F</i>	7	256, 64, 32, 16, 8, 4, 1	2	209	518	199948	0.62

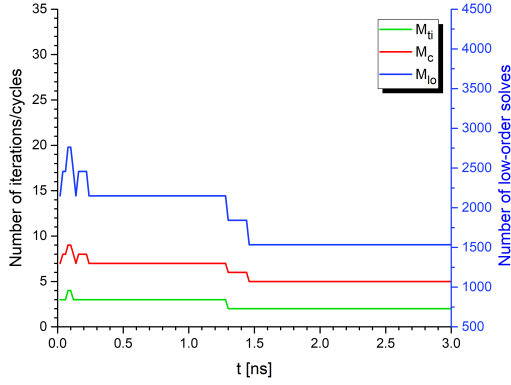




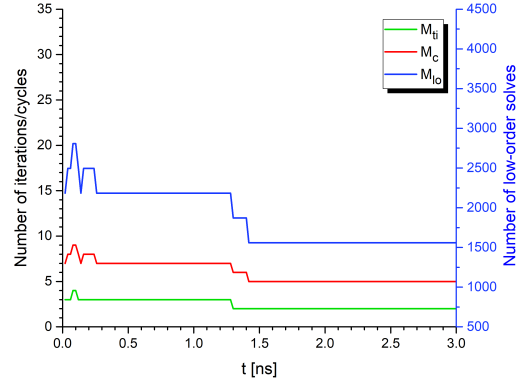
(a)  $\Gamma=2$ ,  $n_\nu^\gamma=256,1$ ,  $V$ -cycle,  $\ell_{max}=4$ .



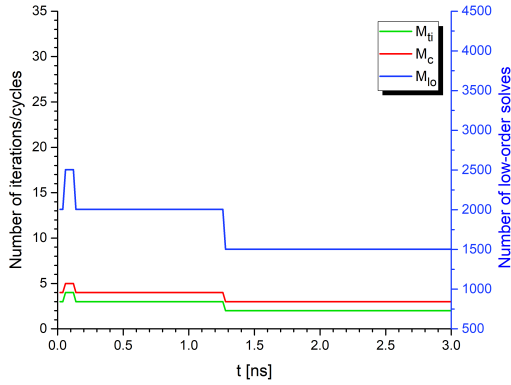
(b)  $\Gamma=3$ ,  $n_\nu^\gamma=256,32,1$ ,  $W$ -cycle,  $\ell_{max}=2$ .



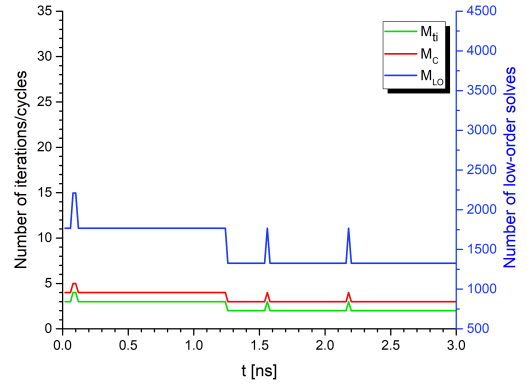
(c)  $\Gamma=4$ ,  $n_\nu^\gamma=256,32,16,1$ ,  $F$ -cycle,  $\ell_{max}=2$ .



(d)  $\Gamma=5$ ,  $n_\nu^\gamma=256,32,16,4,1$ ,  $F$ -cycle,  $\ell_{max}=2$ .

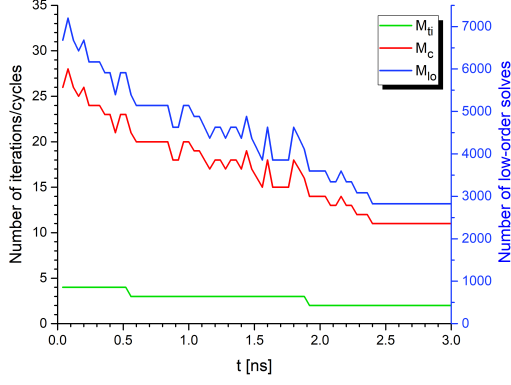


(e)  $\Gamma=6$ ,  $n_\nu^\gamma=256,128,64,32,1$ ,  $F$ -cycle,  $\ell_{max}=1$ .

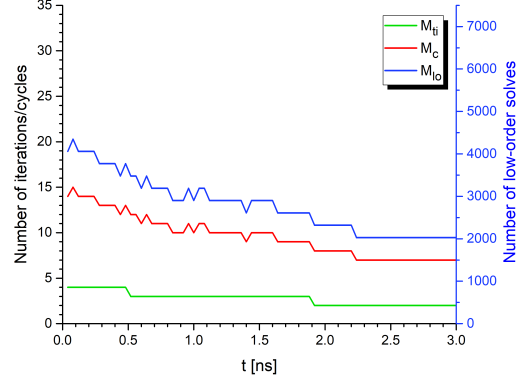


(f)  $\Gamma=7$ ,  $n_\nu^\gamma=256,128,32,16,8,4,1$ ,  $F$ -cycle,  $\ell_{max}=1$ .

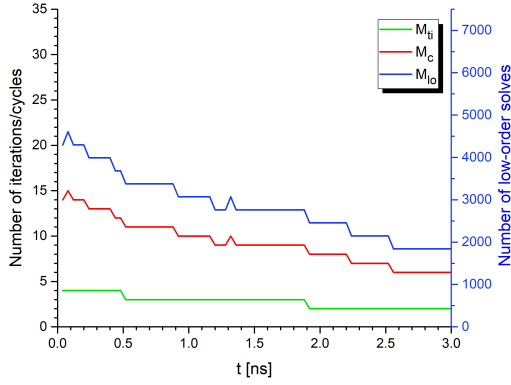
Figure 3: Number of transport iterations ( $M_{ti}$ ), cycles ( $M_c$ ), and low-order solves ( $M_{lo}$ ) at each time step in the FC test with 256 groups and  $\Delta t = 2 \times 10^{-2}$  ns over  $t \in [0, 3$  ns].



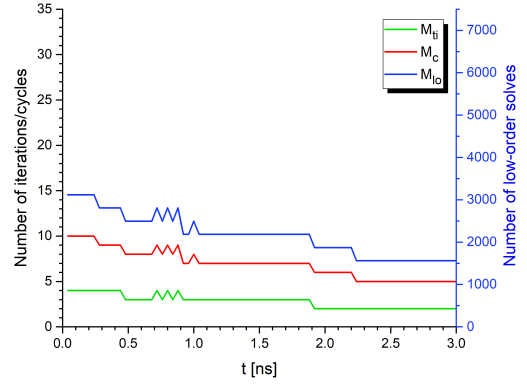
(a)  $\Gamma=2$ ,  $n_\nu^\gamma=256,1$ ,  $V$ -cycle,  $\ell_{max}=6$ .



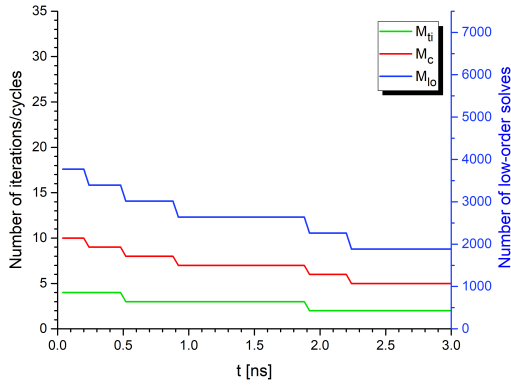
(b)  $\Gamma=3$ ,  $n_\nu^\gamma=256,32,1$ ,  $W$ -cycle,  $\ell_{max}=3$ .



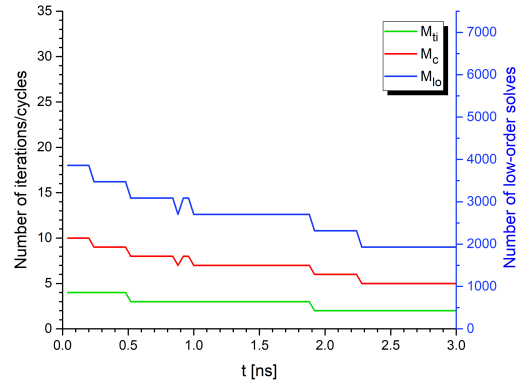
(c)  $F$ -cycle,  $\ell_{max}=3$ ,  $n_\nu^\gamma = 256, 32, 16, 1$ ,  $\Gamma=4$ .



(d)  $\Gamma=5$ ,  $n_\nu^\gamma=256,32,16,4,1$ ,  $F$ -cycle,  $\ell_{max}=2$ .

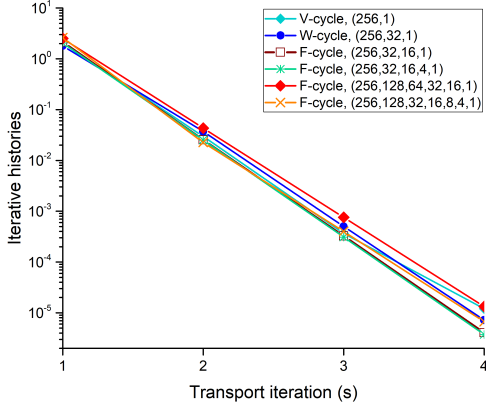


(e)  $\Gamma=6$ ,  $n_\nu^\gamma=256,64,32,16,4,1$ ,  $F$ -cycle,  $\ell_{max}=2$ .

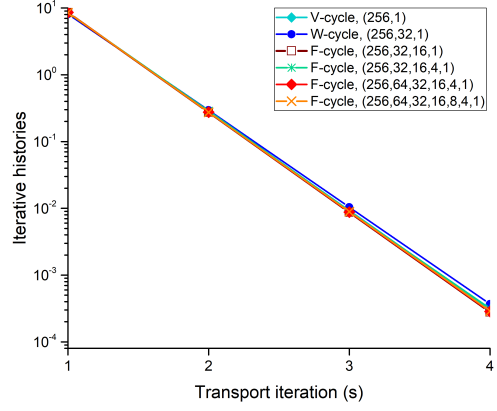


(f)  $\Gamma=7$ ,  $n_\nu^\gamma=256,64,32,16,8,4,1$ ,  $F$ -cycle,  $\ell_{max}=2$ .

Figure 4: Number of transport iterations ( $M_{ti}$ ), cycles ( $M_c$ ), and low-order solves ( $M_{lo}$ ) at each time step in the FC test with 256 groups and  $\Delta t = 4 \times 10^{-2}$  ns over  $t \in [0, 3$  ns].

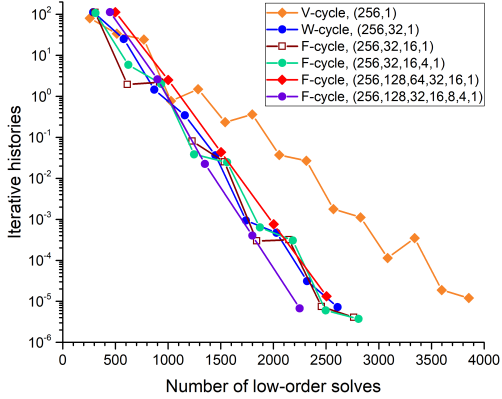


(a)  $\Delta t = 2 \times 10^{-2}$  ns

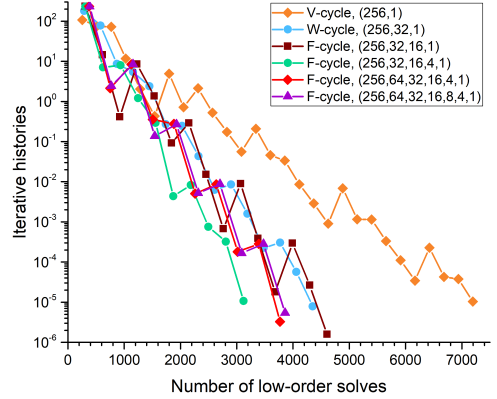


(b)  $\Delta t = 4 \times 10^{-2}$  ns

Figure 5: Convergence of temperature ( $\|\Delta T^{(s)}\|_{\infty}$  [eV]) over transport iterations at  $t = 8 \times 10^{-2}$  ns.



(a)  $\Delta t = 2 \times 10^{-2}$  ns



(b)  $\Delta t = 4 \times 10^{-2}$  ns

Figure 6: Iterative convergence of temperature ( $\|\Delta \tilde{T}^{[k]}\|_{\infty}$  [eV]) over cycles at  $t = 8 \times 10^{-2}$  ns.

## 7. Conclusion

This paper presented iteration transport methods for solving TRT problems in 1D slab geometry. They are derived by nonlinear projection in angular variable and frequency and based on the MLQD method. We developed new nonlinear iterative projection methods for TRT that define the low-order equations on multiple grids in photon frequency. On each transport iteration, the multigroup LOQD equations coupled with the MEB equation are solved iteratively by multigrid-in-frequency algorithms using the  $W$ - and  $F$ -cycles. The obtained results show that the new algorithms accelerate convergence of iterations and reduce computational costs. The behavior

of the iteration algorithms vary depending on the stage in evolution of temperature and radiation energy waves. The algorithms with different cycles and hierarchies of frequency grids can be applied depending on the stage of TRT phenomenon and the value of the time step to further improve effectiveness of iteration methods. This kind of algorithms can be developed for TRT problems with scattering using advanced prolongation operators. Other existing iteration methods for TRT problems can take advantage in applying multigrid in frequency to develop advanced iteration techniques for problems with very large number of frequency groups.

## References

- [1] F. Shu, *The Physics of Astrophysics*, University Science Books, 1991.
- [2] R. P. Drake, *High Energy Density Physics: Fundamentals, Inertial Fusion and Experimental Astrophysics*, Springer, 2006.
- [3] F. Graziani, *Computational Methods in Transport*, Springer, 2004.
- [4] S. Chandrasekhar, *Radiative transfer*, Dover Publications, New York, 1960.
- [5] Y. B. Zeldovich, Y. P. Razier, *Physics of Shock Waves and High Temperature Hydrodynamic Phenomena*, Academic, New York, 1966.
- [6] D. Mihalas, B. Weibel-Mihalas, *Foundation of Radiation Hydrodynamics*, Oxford University Press, 1984.
- [7] J. A. Fleck, J. D. Cummings, An implicit monte carlo scheme for calculating time and frequency dependent nonlinear radiation transport, *Journal of Computational Physics* 8 (1971) 313–342.
- [8] E. W. Larsen, A grey transport acceleration method for time-dependent radiative transfer problems, *Journal of Computational Physics* 78 (1988) 459–480.
- [9] R. E. Alcouffe, B. A. Clark, E. W. Larsen, The diffusion-synthetic acceleration of transport iterations, with application to a radiation hydrodynamics problem, in: *Multiple Time Scales*, Academic Press, 1985, pp. 73–11.
- [10] J. E. Morel, E. W. Larsen, M. K. Matzen, A synthetic acceleration scheme for radiative diffusion calculations, *J. Quant. Spectrosc. Radiat. Transfer* 34 (1985) 243–261.
- [11] J. E. Morel, T.-Y. B. Yang, J. S. Warsa, Linear multifrequency-grey acceleration recast for preconditioned Krylov iterations, *Journal of Computational Physics* 227 (2007) 244–263.
- [12] A. T. Till, M. L. Adams, J. E. Morel, Application of nonlinear Krylov acceleration to radiative transfer problems, in: *Proc. of Int. Conf. on Math. and Comp., M&C 2013*, Sun Valley, Idaho, Spain, 2013, pp. 2690–2701.
- [13] V. Y. Gol'din, A quasi-diffusion method of solving the kinetic equation, *Comp. Math. and Math. Phys.* 4 (1964) 136–149.
- [14] V. Y. Gol'din, On mathematical modeling of problems of non-equilibrium transfer in physical systems, in: *Modern Problems of Mathematical Physics and Computational Mathematics*, Nauka, Moscow, 1982, pp. 113–127, in Russian.
- [15] L. H. Auer, D. Mihalas, On the use of variable Eddington factors in non-LTE stellar atmospheres computations, *Monthly Notices of the Royal Astronomical Society* 149 (1970) 65–74.
- [16] D. Y. Anistratov, E. W. Larsen, Nonlinear and linear  $\alpha$ -weighted methods for particle transport problems, *Journal of Computational Physics* 173 (2001) 664–684.
- [17] L. Roberts, D. Y. Anistratov, Nonlinear weighted flux methods for solving the transport equation in 2D Cartesian geometry, *Nuclear Science and Engineering* 165 (2010) 133–148.
- [18] K. S. Smith, Nodal Method Storage Reduction by Nonlinear Iteration, *Trans. Am. Nucl. Soc.* 44 (1984) 265.
- [19] K. Smith, J. R. III, Full-core 2-D LWR core calculations with CASMO-4E, in: *Int. Conf. on the New Frontiers of Nucl. Tech.: Reactor Phys., Safety and High-Performance Computing*, 2002, Seoul, Korea, October 7-10.
- [20] N. Z. Cho, G. S. Lee, C. J. Park, Partial current-based CMFD acceleration of the 2D/1D fusion method for 3D whole-core transport calculations, *Transaction of the American Nuclear Society* 88 (2003) 594–596.
- [21] V. Y. Gol'din, B. N. Chetverushkin, Methods of solving one-dimensional problems of radiation gas dynamics, *USSR Comp. Math. and Math. Phys.* 12 (1972) 177–189.
- [22] V. V. Gorskii, S. T. Surzhikov, Use of the semimoment method to solve the shock layer radiative heat-transfer problem, *Journal of Engineering Physics* 42 (1982) 108–111.
- [23] V. Y. Gol'din, D. A. Gol'dina, A. V. Kolpakov, A. V. Shil'kov, Mathematical modeling of hydrodynamics processes with high-energy density radiation, *Problems of Atomic Sci. & Eng.: Methods and Codes for Numerical Solution of Math. Physics Problems* 2 (1986) 59–88, in Russian.

- [24] K.-L. A. Winkler, M. L. Norman, D. Mihalas, Implicit adaptive-grid radiation hydrodynamics, in: *Multiple Time Scales*, Academic Press, 1985, pp. 145–184.
- [25] D. Y. Anistratov, E. N. Aristova, V. Y. Gol'din, A nonlinear method for solving problems of radiation transfer in a physical system, *Mathematical Modeling* 8 (1996) 3–28, in Russian.
- [26] E. N. Aristova, V. Y. Gol'din, A. V. Kolpakov, Multidimensional calculations of radiation transport by nonlinear quasi-diffusion method, in: *Proc. of Int. Conf. on Math. and Comp., M&C 1999*, Madrid, Spain, 1999, pp. 667–676.
- [27] H. Park, D. A. Knoll, R. M. Rauenzahn, A. B. Wollaber, J. D. Densmore, Moment-based, multiscale solution approach for thermal radiative transfer problems, *Transport Theory and Statistical Physics* 41 (2012) 284–303.
- [28] B. C. Yee, A. B. Wollaber, T. S. Haut, H. Park, A stable 1D multigroup high-order low-order method, *Journal of Computational and Theoretical Transport* 46 (2016) 46–76.
- [29] D. Y. Anistratov, Stability analysis of a multilevel quasidiffusion method for thermal radiative transfer problems, *Journal of Computational Physics* 376 (2019) 186–209.
- [30] L. R. Cornejo, D. Y. Anistratov, Nonlinear diffusion acceleration method with multigrid in energy for k-eigenvalue neutron transport problems, *Nuclear Science and Engineering* 184 (2016) 514–526.
- [31] L. R. Cornejo, D. Y. Anistratov, K. Smith, Iteration methods with multigrid in energy for eigenvalue neutron diffusion problems, *Nuclear Science and Engineering* 193 (2019) 803–827.
- [32] L. R. Cornejo, D. Y. Anistratov, Multilevel algorithms with projection and prolongation over elements of the phase space for k-eigenvalue transport problems, in: *Proc. of Int. Conf. on Mathematics and Computational Methods Applied to Nuclear Science and Engineering (M&C 2019)*, 2019, pp. 2391–2400, Portland, OR, August 25.
- [33] B. Lee, Space-angle-energy multigrid methods for  $S_n$  discretizations of the multi-energetic boltzmann equation, *Numerical Linear Algebra with Applications* 19 (2012) 773–795.
- [34] A. S. Moore, T. M. Guymer, J. Morton, B. Williams, J. L. Kline, N. Bazin, C. Bentley, S. Allan, K. Brent, A. J. Comley, K. Flippo, J. Cowan, J. M. Taccetti, K. Mussack-Tamashiro, D. W. Schmidt, C. E. Hamilton, K. Obrey, N. E. Lanier, J. B. Workman, R. M. Stevenson, Characterization of supersonic radiation diffusion waves, *Journal of Quantitative Spectroscopy and Radiative Transfer* 159 (2015) 19–28.
- [35] U. Trottenberg, C. Oosterlee, A. Schuller, *Multigrid*, Academic Press, San Diego San Francisco New York Boston London Sydney Tokyo, 2000.
- [36] D. A. Knoll, R. B. Lowrie, J. E. Morel, Numerical analysis of time integration errors for nonequilibrium radiation diffusion, *Journal of Computational Physics* 226 (2007) 1332–1347.
- [37] M. L. Adams, Subcell balance methods for radiative transfer on arbitrary grids, *Transport Theory and Statistical Physics* 26 (1997) 385–431.